Thoracic Staging in Lung Cancer: Prospective Comparison of ^{18}F-FDG PET/MR Imaging and ^{18}F-FDG PET/CT

Philipp Heusch*[1,2], Christian Buchbender*[1], Jens Köhler[3], Felix Nensa[2], Thomas Gauler[3], Benedikt Gomez[4], Henning Reis[5], Georgios Stamatis[6], Hilmar Kühl[2], Verena Hartung[4], and Till A. Heusner[1,2]

[1]University Dusseldorf, Medical Faculty, Department of Diagnostic and Interventional Radiology, Dusseldorf, Germany; [2]University Duisburg-Essen, Medical Faculty, Department of Diagnostic and Interventional Radiology and Neuroradiology, Essen, Germany; [3]University Duisburg-Essen, Medical Faculty, Department of Medical Oncology, Essen, Germany; [4]University Duisburg-Essen, Medical Faculty, Department of Nuclear Medicine, Essen, Germany; [5]University Duisburg-Essen, Medical Faculty, Institute of Pathology and Neuropathology, Essen, Germany; and [6]Thoracic Surgery and Endoscopy, Ruhrlandklinik, University Duisburg-Essen, Essen, Germany

Therapeutic decisions in non–small cell lung cancer (NSCLC) patients depend on the tumor stage. PET/CT with ^{18}F-FDG is widely accepted as the diagnostic standard of care. The purpose of this study was to compare a dedicated pulmonary ^{18}F-FDG PET/MR imaging protocol with ^{18}F-FDG PET/CT for primary and locoregional lymph node staging in NSCLC patients using histopathology as the reference. **Methods:** Twenty-two patients (12 men, 10 women; mean age ± SD, 65.1 ± 9.1 y) with histopathologically confirmed NSCLC underwent ^{18}F-FDG PET/CT, followed by ^{18}F-FDG PET/MR imaging, including a dedicated pulmonary MR imaging protocol. T and N staging according to the seventh edition of the American Joint Committee on Cancer staging manual was performed by 2 readers in separate sessions for ^{18}F-FDG PET/CT and PET/MR imaging, respectively. Results from histopathology were used as the standard of reference. The mean and maximum standardized uptake value (SUV_{mean} and SUV_{max}, respectively) and maximum diameter of the primary tumor was measured and compared in ^{18}F-FDG PET/CT and PET/MR imaging. **Results:** PET/MR imaging and ^{18}F-FDG PET/CT agreed on T stages in 16 of 16 of patients (100%). All patients were correctly staged by ^{18}F-FDG PET/CT and PET/MR (100%), compared with histopathology. There was no statistically significant difference between ^{18}F-FDG PET/CT and ^{18}F-FDG PET/MR imaging for lymph node metastases detection ($P = 0.48$). For definition of thoracic N stages, PET/MR imaging and ^{18}F-FDG PET/CT were concordant in 20 of 22 patients (91%). PET/MR imaging determined the N stage correctly in 20 of 22 patients (91%). ^{18}F-FDG PET/CT determined the N stage correctly in 18 of 22 patients (82%). The mean differences for SUV_{mean} and SUV_{max} of NSCLC in ^{18}F-FDG PET/MR imaging and ^{18}F-FDG PET/CT were 0.21 and −5.06. These differences were not statistically significant ($P > 0.05$). The SUV_{mean} and SUV_{max} measurements derived from ^{18}F-FDG PET/CT and ^{18}F-FDG PET/MR imaging exhibited a high correlation ($R = 0.74$ and 0.86, respectively; $P < 0.0001$). Size measurements showed an excellent correlation between ^{18}F-FDG PET/MR imaging and ^{18}F-FDG PET/CT ($R = 0.99$; $P < 0.0001$). The lower and upper limits of agreement between ^{18}F-FDG PET/CT and ^{18}F-FDG PET/MR imaging using Bland–Altman analysis were −2.34 to 3.89 for SUV_{mean}, −7.42 to 4.40 for SUV_{max}, and −0.59 to 0.83 for the tumor size, respectively. **Conclusion:** ^{18}F-FDG PET/MR imaging using a dedicated pulmonary MR imaging protocol, compared with ^{18}F-FDG PET/CT, does not provide advantages in thoracic staging in NSCLC patients.

Key Words: oncology; general; PET/CT; PET/MRI; ^{18}F-FDG PET/CT; ^{18}F-FDG PET/MR imaging; ^{18}F-FDG PET/MRI; NSCLC

J Nucl Med 2014; 55:373–378
DOI: 10.2967/jnumed.113.129825

Lung cancer is the most frequently diagnosed cancer, with one of the highest mortality rates worldwide (*1*). Approximately 80% of all lung malignancies are classified as non–small cell lung cancer (NSCLC) (*1*). Treatment concepts are based on tumor stage and include surgery, radiation, or chemotherapy. Optimal staging is needed to limit surgery or multimodality treatment to only those patients who might benefit from such therapy. Because of its high diagnostic accuracy in the detection and staging of the primary lung tumor and distant metastases (*2,3*), ^{18}F-FDG PET/CT is accepted as the first-line staging tool in patients who qualify for potentially curative treatment. However, staging of the primary tumor using ^{18}F-FDG PET/CT can be challenging. In particular, parenchymal changes in the postobstructive lung tissue and infiltration of the adjacent pleural and mediastinal structures might lead to errors in T staging performance (*4,5*).

The mediastinal nodal stage is the most important prognostic factor concerning the chance for and the duration of survival (*6*). Sensitivity and specificity for the detection of mediastinal lymph node metastases with chest CT is limited. ^{18}F-FDG PET/CT suffers from a high number of false-positive mediastinal lymph nodes caused by its low specificity in distinguishing inflammatory and granulomatous lymph nodes from lymph node metastases (*7–9*). This results in a high negative predictive value for detection of thoracic lymph node metastases of ^{18}F-FDG PET/CT, but a lower positive predictive value requires verification with invasive techniques such as optical bronchoscopy or biopsy, endobronchial ultrasound–guided transbronchial needle aspiration (EBUS-TBNA), or mediastinoscopy (*10–16*).

Recently MR imaging has been proven to provide advantages in T staging and N staging performance when compared with ^{18}F-FDG PET/CT (*17,18*). Whole-body (WB) integrated ^{18}F-FDG PET/MR imaging scanners enable simultaneous acquisition and accurate spatial coregistration of PET and MR images (*19,20*). It is

Received Jul. 24, 2013; revision accepted Oct. 10, 2013.
For correspondence or reprints contact: Philipp Heusch, University Dusseldorf, Medical Faculty, Department of Diagnostic and Interventional Radiology, Moorenstrasse 5, 40225 Dusseldorf, Germany.
E-mail: Philipp.heusch@med.uni-duesseldorf.de
*Contributed equally to this work.
Published online Feb. 6, 2014.

expected that MR imaging in combination with PET will provide a new quality in functional cancer imaging (*21*), mainly due to the combination of functional MR and PET information.

In a pilot study with 10 patients, Schwenzer et al. have recently highlighted the feasibility of simultaneous PET/MR for the assessment of pulmonary masses showing a similar lesion characterization and tumor stage, compared with ^{18}F-FDG PET/CT (*22*), but no dedicated lung MR imaging protocol and no histopathologic reference standard was used in this early study. Hence, the purpose of the present study was to test whether ^{18}F-FDG PET/MR imaging, including a dedicated pulmonary MR imaging protocol, provides a higher diagnostic value than ^{18}F-FDG PET/CT for thoracic T and N staging in NSCLC patients using histopathologic findings as the reference.

MATERIALS AND METHODS

Patients

In 22 consecutive patients (12 men, 10 women; mean age ± SD, 65.1 ± 9.1 y) with histopathologically confirmed NSCLC, a thoracic ^{18}F-FDG PET/MR imaging protocol was performed according to current MR imaging guidelines (*23*) after routine clinical ^{18}F-FDG PET/CT. Tumor histopathology was determined from samples obtained with endobronchial ultrasound biopsy, or thoracotomy in every patient. To determine the adequate N stage, 17 patients received thoracic surgery, 3 patients received a complete thoracic mediastinoscopy, and 2 patients received EBUS-TBNA, respectively. The T stage was assessed by thoracotomy and resection of the primary tumor. Histopathologic workup was conducted according to institutional standards, current diagnostic criteria of the World Health Organization/International Agency for Research on Cancer were applied, and staging was performed according to the TNM Classification of Malignant Tumors (seventh edition). Fourteen patients had adenocarcinomas, 5 patients had squamous cell carcinomas, and 3 patients had large cell carcinomas. The institutional review board approved this prospective study and all subjects signed a written informed consent.

PET/CT Imaging

WB ^{18}F-FDG PET/CT scans were obtained on an mCT PET/CT scanner (Siemens Molecular Imaging). All patients had blood glucose levels below 150 mg/dL at the time of ^{18}F-FDG injection. ^{18}F-FDG (300 ± 45 MBq) was intravenously injected 60 min before the scan. The contrast-enhanced CT scan was obtained at baseline breathing with the following parameters: iodinated contrast agent injection (100 mL) (Ultravist 300; Bayer Healthcare); flow rate, 2 mL/s, followed by a flush of 2.5 mL of saline/s start delay, 70 s; caudocranial scan direction; field of view (FOV), skull base to upper thighs; 120 kV; automatic mA/s adjustment (Care Dose 4D [Siemens AG, Healthcare Section]; preset, 210 mAs); slice thickness, 5 mm; increment, 5 mm; pitch, 1. The contrast-enhanced CT scan was followed by a deep-inspiration CT scan of the lungs with the following parameters: caudocranial scan direction; FOV, 300 mm; 100 kV; automatic mA/s adjustment (Care Dose 4D); slice thickness, 3 mm; increment, 2 mm; pitch, 1.2. The PET scan parameters were 3-dimensional (3D) mode; 2-min emission time per bed position (45% overlap); reconstruction according to the ordered-subsets expectation maximization algorithm, with 4 iterations and 8 subsets; 3D gaussian filter, 4.0 mm, full width at half maximum (FWHM); scatter correction. The attenuation correction was based on the portal venous phase of the WB CT.

PET/MR Imaging

WB ^{18}F-FDG PET/MR imaging was performed on a Magnetom Biograph mMR (Siemens Healthcare). ^{18}F-FDG PET/MR imaging was performed after ^{18}F-FDG PET/CT, with a mean delay of 85 ± 34 min. The FOV contained the body volume from the head to the thighs. PET acquisition time was 20 min for the thorax. PET images were reconstructed using the iterative algorithm ordered-subsets expectation maximization, 3 iterations and 21 subsets; gaussian filter, 4.0 mm in full width at half maximum; attenuation and scatter correction. A dedicated mMR head and neck coil and, depending on the patients' height, up to 4 mMR body flex coils were used for MR imaging. MR imaging was performed simultaneously with PET imaging using the following sequence protocol for each bed position:

- A coronal 3D volume-interpolated gradient echo (VIBE) sequence (repetition time [TR], 3.6 ms; echo time 1 [TE1], 1.23 ms; TE2, 2.46 ms; slice thickness, 3.12 mm; FOV, 500 mm for DIXON-based attenuation correction).
- A coronal T2-weighted steady-state free precession (TrueFISP) sequence of the thorax (TR, 3.75 ms; TE, 1.64 ms; matrix size, 320; slice thickness, 6 mm; FOV, 330 mm; generalized auto calibrating partially parallel acquisition [GRAPPA]; acceleration factor, 2).
- A transversal T2-weighted blade turbo spin echo sequence of the thorax in breath-hold technique (TR, 4,360 ms; TE, 160 ms; matrix size, 384; slice thickness, 5 mm; FOV, 400 mm; GRAPPA; acceleration factor, 2).
- Transversal echo planar imaging diffusion-weighted imaging (TR, 10,500 ms; TE, 78 ms; diffusion weightings [b-values] 0, 500, and 1000 s/mm^2; matrix size, 160; slice thickness, 5 mm; 40 slices; FOV, 450 mm; GRAPPA; acceleration factor, 2; 2 averages).
- Transversal T1-weighted fast low angle shot gradient echo sequence (FLASH) (TR, 1,510 ms; TE, 2.15 ms; inversion time [TI], 1,200 ms; matrix size, 320; slice thickness, 5 mm; FOV, 400 mm; GRAPPA; acceleration factor, 2).
- Coronal half Fourier acquisition single-shot turbo spin echo sequence of the thorax (TR, 649 ms; TE, 51 ms; matrix size, 320; slice thickness, 6 mm; FOV, 330 mm; GRAPPA; acceleration factor, 2).
- Coronal 3D VIBE sequence of the thorax (TR, 3.66 ms; TE, 1.29 ms; matrix size, 192; slice thickness, 4 mm; FOV, 350 mm; GRAPPA; acceleration factor, 2).
- Coronal 3D VIBE sequence of the thorax after intravenous administration of gadolinium with a delay of 2 min (TR, 3.67 ms; TE, 1.29 ms; matrix size, 192; slice thickness, 4 mm; FOV, 350 mm; GRAPPA; acceleration factor, 2).
- Transversal fat-saturated T1-weighted FLASH after intravenous administration of gadolinium of the whole body (TR, 1,700 ms; TE, 3.33 ms; TI, 1,200 ms; matrix size, 256; slice thickness, 7.5 mm; FOV, 450 mm; GRAPPA; acceleration factor, 2).
- Coronal 2-dimensional turbo inversion recovery sequence with magnitude with short TI for fat suppression in free-breathing of the whole body (TR, 3,190 ms; TE, 55 ms; matrix size, 384; slice thickness, 5 mm; FOV, 450 mm; GRAPPA; acceleration factor, 2).

^{18}F-FDG PET/MR image fusion was performed for the postcontrast T1-weighted VIBE images, the postcontrast T1-weighted FLASH sequence, and the T2-weighted blade images.

Image Analysis. T and N staging according to the seventh edition of the American Joint Committee on Cancer staging manual was performed by 2 readers with 3 and 4 y of experience in MR imaging and 2 and 3 y of experience in hybrid ^{18}F-FDG PET/CT imaging, respectively. Both readers were aware of the patients' diagnosis of NSCLC but were masked to all other clinical data. ^{18}F-FDG PET/CT and ^{18}F-FDG PET/MR images were analyzed separately, in a separate session and in random order using a picture-archiving and communication system (Centricity; GE Healthcare) and dedicated viewing software for hybrid imaging (Syngo.via;

Siemens, Healthcare Sector). There was an interval of at least 4 wk was in between the reading of the ^{18}F-FDG PET/CT and ^{18}F-FDG PET/MR imaging datasets. Discrepancies between both readers were resolved by consensus reading of both readers in a separate session. In fused ^{18}F-FDG PET/CT and PET/MR images, a polygonal region of interest was placed, respectively, covering the primary tumor to determine the SUV_{mean}, SUV_{max}.

The assessment of the primary tumor and of lymph node metastases with ^{18}F-FDG PET/CT and ^{18}F-FDG PET/MR imaging was based on qualitative and quantitative analyses. ^{18}F-FDG PET/CT and ^{18}F-FDG PET/MR imaging data were evaluated qualitatively for regions of focally increased tracer uptake by visual comparison of the lesion's signal to the ^{18}F-FDG uptake of the liver parenchyma in PET (*15*). Furthermore, for ^{18}F-FDG PET/CT lymph nodes were graded as benign or malignant based on these functional criteria and based on their size (*24*). Determination of lymph node size was based on measurement of the short-axis diameter. Region-specific size criteria were applied when assessing lymph nodes for malignancy (*25*). Central necrosis was considered as a sign of malignant tumor spread independent of lymph node size. For ^{18}F-FDG PET/MR imaging, readers were instructed to identify all malignant lymph nodes according to the following criteria: elevated short-axis diameter, pathologic signal intensity (heterogeneous vs. homogeneous), central necrosis, shape (smooth vs. irregular), contrast enhancement, high signal on b-1,000 diffusion-weighted images with low signal intensity on corresponding ADC maps, and focal ^{18}F-FDG uptake (*7,26*).

PET images were assessed with and without attenuation correction of the PET data to avoid false-positive findings due to attenuation-correction artifacts.

Statistics

Statistical analysis was performed using SPSS 21 (SPSS Inc.). Data are presented as mean ± SD. Descriptive analysis was used for SUV_{mean} and SUV_{max} of the primary tumor. Interreader agreement for ^{18}F-FDG PET/MR imaging and ^{18}F-FDG PET/CT was assessed in terms of κ coefficients. Pearson correlation coefficients were calculated to compare the SUV_{mean}, SUV_{max}, and maximum diameter of the primary tumor. Sensitivity, specificity, positive predictive value, negative predictive value, and diagnostic accuracy for presence of mediastinal lymph node metastases were calculated for ^{18}F-FDG PET/MR imaging and ^{18}F-FDG PET/CT, respectively. A McNemar test was performed to investigate differences in diagnostic performance between the different imaging procedures; for comparison of the mean difference between SUV_{mean} and SUV_{max} in ^{18}F-FDG PET/CT and ^{18}F-FDG PET/MR imaging, a Wilcoxon signed-rank test was applied. A P value of less than 0.05 was considered to indicate statistical significance. Furthermore, interdevice agreement between PET images acquired on the ^{18}F-FDG PET/CT and ^{18}F-FDG PET/MR imaging scanners for SUV_{mean}, SUV_{max}, and the size of the primary tumor was analyzed using Bland–Altman plots.

RESULTS

^{18}F-FDG PET/CT and ^{18}F-FDG PET/MR imaging acquisitions were completed successfully in all 22 patients. No sources of obvious artifacts or systematic errors were seen in PET data acquired on the PET/MR imaging scanner.

For ^{18}F-FDG PET/CT and ^{18}F-FDG PET/MR imaging, a high interobserver agreement could be demonstrated for T staging ($\kappa = 0.92$). ^{18}F-FDG PET/CT and ^{18}F-FDG PET/MR imaging agreed in T staging in 16 of 16 of patients (100%). Compared with resection specimens as the reference standard, the primary tumor was correctly staged by ^{18}F-FDG PET/CT and PET/MR in all 16 patients (100%) (Fig. 1).

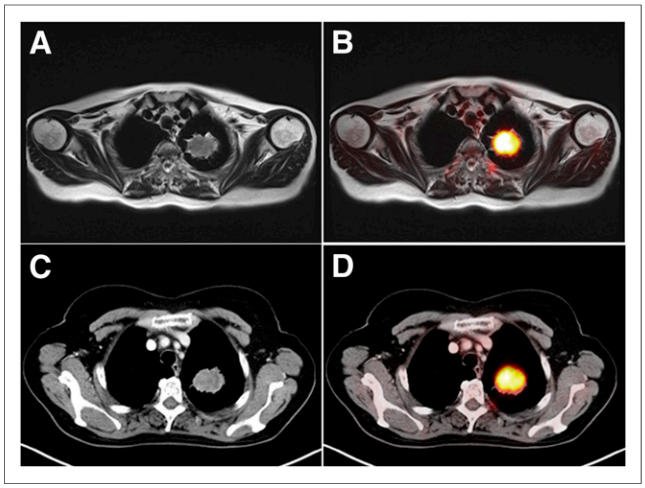

FIGURE 1. ^{18}F-FDG–avid, histologically proven NSCLC in left upper lobe of 59-y-old female patient on T2-weighted blade MR image with measured maximum diameter of 3.7 cm (A) and on fused ^{18}F-FDG PET/MR image (B). Identical tumor mass of same patient in left upper lobe on CT image with measured maximum diameter of 3.8 cm (C) and on ^{18}F-FDG PET/CT image (D). Primary tumor was correctly staged as T2a tumor in ^{18}F-FDG PET/MR imaging and ^{18}F-FDG PET/CT.

For N staging, a κ value of 0.92 indicated a good agreement between the 2 observers using ^{18}F-FDG PET/CT and ^{18}F-FDG PET/MR imaging, respectively.

For thoracal N staging, ^{18}F-FDG PET/MR imaging and ^{18}F-FDG PET/CT were concordant in 20 of 22 patients (91%). ^{18}F-FDG PET/MR imaging correctly rated the N stage in 20 of 22 patients (91%). ^{18}F-FDG PET/CT correctly rated the N stage in 18 of 22 patients (82%). In 1 patient, discrepant N stages in ^{18}F-FDG PET/MR imaging and ^{18}F-FDG PET/CT were due to an ^{18}F-FDG PET–positive lymph node in ^{18}F-FDG PET/CT that did not show any tracer uptake in the ^{18}F-FDG PET/MR imaging examination (histopathologically N0) (Fig. 2). In another case, a malignant lymph node was detected only by ^{18}F-FDG PET/MR imaging, whereas in ^{18}F-FDG PET/CT no pathologic ^{18}F-FDG uptake could be seen. In 1 case, in ^{18}F-FDG PET/MR imaging and in ^{18}F-FDG PET/CT an enlarged, ^{18}F-FDG PET–positive lymph node was falsely rated as malignant (histopathologically N0) (Fig. 3). Both image modalities missed a malignant supraclavicular lymph node (histopathologically N3) that did not show any tracer uptake in both examinations but was rated malignant in histopathology. Sensitivity, specificity, positive predictive value, negative predictive value, and diagnostic accuracy for the detection of mediastinal lymph node metastases were 88%, 93%, 88%, 93%, and 91%, respectively, for ^{18}F-FDG PET/MR imaging and 75%, 86%, 75%, 86%, and 82%, respectively, for ^{18}F-FDG PET/CT. There was no statistically significant difference between ^{18}F-FDG PET/CT and ^{18}F-FDG PET/MR imaging for lymph node metastases detection ($P = 0.48$).

The SUV_{max} of NSCLC was 12.0 ± 5.7 for ^{18}F-FDG PET/MR imaging and 10.5 ± 5.3 for ^{18}F-FDG PET/CT. The SUV_{max} measurements derived from ^{18}F-FDG PET/CT and ^{18}F-FDG PET/MR imaging exhibited a high correlation ($R = 0.86$; $P < 0.0001$). The SUV_{mean} of NSCLC was 3.4 ± 1.5 for ^{18}F-FDG PET/MR imaging and 4.2 ± 2.3 for ^{18}F-FDG PET/CT. The SUV_{mean} measurements derived from ^{18}F-FDG PET/CT and ^{18}F-FDG PET/MR imaging exhibited a good correlation ($R = 0.74$; $P < 0.0001$). The mean difference for SUV_{mean} and SUV_{max}

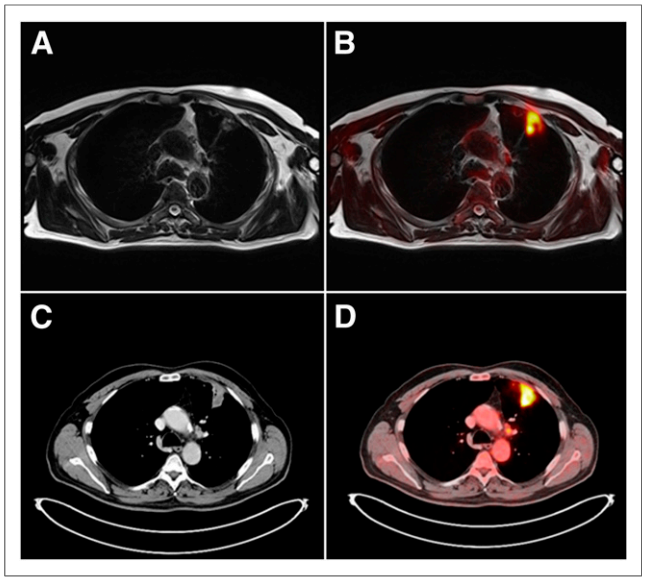

FIGURE 2. Not pathologically enlarged suprahilar lymph node on left side in 71-y-old male patient with histologically proven NSCLC in left upper lung with short-axis diameter of 0.7 cm on T2-weighted blade MR image (A) and on fused ^{18}F-FDG PET/MR image (B). Identical suprahilar lymph node of same patient on CT image with short-axis diameter of 0.7 cm (C) and on ^{18}F-FDG PET/CT image (D). Histopathologically, lymph node was rated as benign (inflammatory changes).

of NSCLC in ^{18}F-FDG PET/MR imaging and ^{18}F-FDG PET/CT was 0.21 ($P = 0.17$) and −5.06 ($P = 0.08$). These differences were not statistically significant. The measured size of the primary tumor was 4.3 ± 2.7 cm in ^{18}F-FDG PET/CT and 4.2 ± 2.6 cm in ^{18}F-FDG PET/MR imaging. Size measurements showed an excellent correlation between ^{18}F-FDG PET/MR imaging and ^{18}F-FDG PET/CT ($R = 0.99$; $P < 0.0001$). When Bland–Altman analysis was used, the lower and upper limits of agreement between ^{18}F-FDG PET/CT and ^{18}F-FDG PET/MR imaging were −7.42 to 4.40 for SUV_{max} (Fig. 4), −2.34 to 3.89 for SUV_{mean}, and −0.59 to 0.83 for the tumor size, respectively (Fig. 5).

DISCUSSION

In potentially resectable NSCLC patients, accurate T and N staging is mandatory. For the assessment of pulmonary masses with ^{18}F-FDG PET/MR imaging, the technical feasibility and a good diagnostic image quality has been previously demonstrated (*22*). Furthermore, it has been recently stated that ^{18}F-FDG PET/MR imaging equals ^{18}F-FDG PET/CT for staging and quantitative assessment of mediastinal NSCLC lymph node metastases (*27*). However, most of these findings have not been proven by studies using a dedicated lung MR protocol and histopathology as reference. This is, to our knowledge, the first study that confirms the diagnostic value of dedicated pulmonary ^{18}F-FDG PET/MR imaging for thoracic T and N staging in NSCLC patients using tumor histopathology and histologic results of systematic lymphadenectomy or mediastinoscopy as the reference.

Regarding the diagnostic accuracy of ^{18}F-FDG PET/CT and MR imaging in NSCLC staging, multiple contradictory results can be found in the literature. In a previous study comparing the diagnostic performance of ^{18}F-FDG PET/CT and WB MR imaging, ^{18}F-FDG PET/CT and 3.0-T WB MR imaging offered comparable efficacy and accuracy for NSCLC staging (*26*). In contrast to the results of Ohno et al., who recently demonstrated that MR imaging is even more accurate and more sensitive than ^{18}F-FDG PET/CT for the qualitative and quantitative assessment of N stage disease in patients with NSCLC (*18*), Plathow et al. stated that ^{18}F-FDG PET/CT provides advantages in N staging over WB MR imaging, whereas MR imaging offers advantages in T staging (*17*). In the latter study, MR imaging had a significant tendency to understage NSCLC concerning N stage because of the lack of metabolic information (*17*). On the basis of the reported studies, it has been hypothesized that the combination of a newly available simultaneous acquisition of PET data and MR imaging might improve thoracic staging in NSCLC patients. In the present study, a comparable good diagnostic performance regarding T and N staging of NSCLC patients was found for hybrid ^{18}F-FDG PET/MR imaging and ^{18}F-FDG PET/CT. In contrast to a previous study by Schwenzer et al., the primary tumor was correctly staged by ^{18}F-FDG PET/CT and ^{18}F-FDG PET/MR imaging in 100%, compared with histopathology. It has to be stressed that compared with Schwenzer et al., we did not have any contestable cases in which the infiltration of adjacent structures could not be excluded at ^{18}F-FDG PET/CT, whereas ^{18}F-FDG PET/MR imaging confirmed an intact mediastinal fat stripe adjacent to the tumor. In fact, regarding T staging the detection of infiltration of the adjacent structures (e.g., mediastinum, pleura) is supposed to be one potential advantage of PET/MR, compared with ^{18}F-FDG PET/CT. In our study, tumor size correlated well between ^{18}F-FDG PET/CT and ^{18}F-FDG PET/MR imaging. Primary tumors due to advanced tumor stages of the enrolled patients were relatively large in this study (^{18}F-FDG PET/CT, 4.3 ± 2.7 cm, and ^{18}F-FDG PET/MR imaging, 4.2 ± 2.6 cm). Therefore, we cannot exclude significant discrepancies in size measurements of smaller NSCLC between ^{18}F-FDG PET/MR imaging and ^{18}F-FDG PET/CT.

For thoracic lymph node metastases detection, we did not find a statistically significant difference for ^{18}F-FDG PET/MR imaging and ^{18}F-FDG PET/CT. For definition of thoracic N stages, ^{18}F-FDG

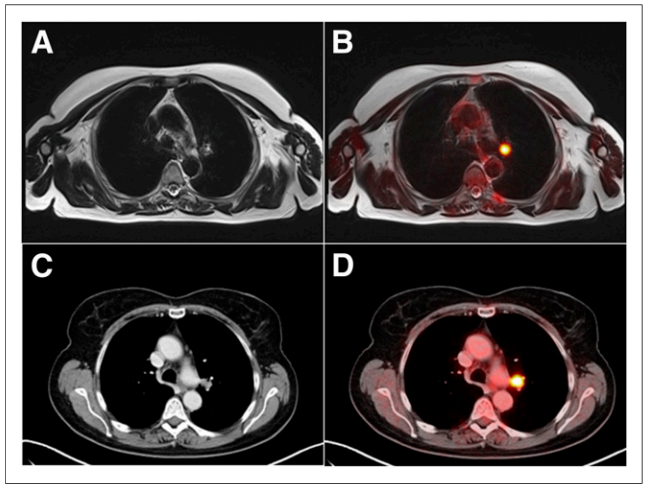

FIGURE 3. Hilar lymph node on left side in 59-y-old female patient with histologically proven NSCLC in left upper lung on T2-weighted blade MR image with short-axis diameter of 1.3 cm (A). This lymph node shows pathologic ^{18}F-FDG uptake on fused ^{18}F-FDG PET/MR image (B). Identical hilar lymph node of same patient on CT image with short-axis diameter of 1.3 cm (C), clearly visible on ^{18}F-FDG PET/CT image (D). Histopathologically, lymph node was rated as benign (inflammatory changes).

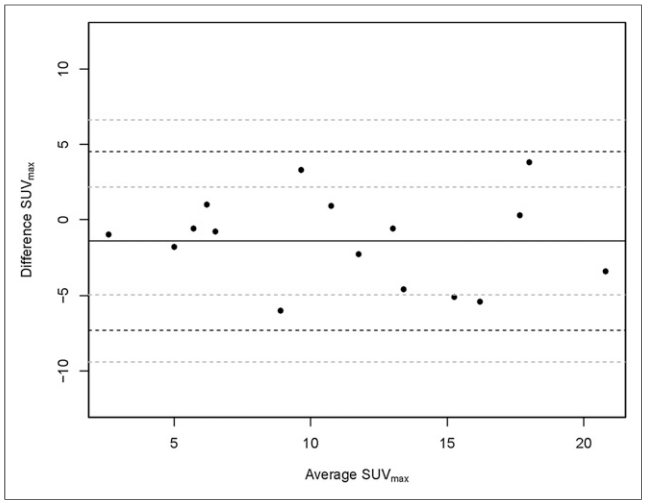

FIGURE 4. Bland–Altman analysis showing lower and upper limits of agreement between ^{18}F-FDG PET/CT and ^{18}F-FDG PET/MR imaging of −7.42 to 4.40 for SUV_{max}.

PET/MR imaging and ^{18}F-FDG PET/CT were concordant in 91% of patients, but compared with our reference standard ^{18}F-FDG PET/MR imaging was correct in 91% whereas ^{18}F-FDG PET/CT was less correct in only 82% of cases. One discrepancy in ^{18}F-FDG PET/MR imaging and ^{18}F-FDG PET/CT staging was caused by an enlarged ^{18}F-FDG PET–positive lymph node in ^{18}F-FDG PET/CT that did not show any tracer uptake in the ^{18}F-FDG PET/MR imaging examination. Histopathology revealed an inflammatory altered lymph node. In another case, a malignant lymph node was detected only by ^{18}F-FDG PET/MR imaging, whereas in ^{18}F-FDG PET/CT no pathologic ^{18}F-FDG uptake could be seen. Histopathologic analysis revealed a malignant lymph node. The latter discrepancy might be explained by the time delay and the resulting increasing tracer uptake into the metastasis, which was then depicted by ^{18}F-FDG PET/MR imaging. This effect could have potentially biased our evaluation, and the reported marginal differences between ^{18}F-FDG PET/MR imaging and ^{18}F-FDG PET/CT for N staging might be overestimated. We did not perform a dual-time-point ^{18}F-FDG PET/CT examination to exclude the effect of time delay of the respective PET measurements. Because patients were studied in a clinical setting and therefore ^{18}F-FDG PET/CT measurements had to be performed at the optimal time point (60 min after injection), we did not perform measurements in reverse order to discriminate the effects of changes in ^{18}F-FDG activity over time from other causes.

In ^{18}F-FDG PET/MR imaging and in ^{18}F-FDG PET/CT an enlarged, ^{18}F-FDG PET–positive lymph node was falsely rated as malignant (histopathologically N0). Both image modalities missed a malignant supraclavicular lymph node (histopathologically N3) that did not show any tracer uptake in both examinations but was rated malignant in histopathology. Although in this study ^{18}F-FDG PET/CT and ^{18}F-FDG PET/MR imaging are comparably good in N staging performance, relying on PET sensitivity only, they suffer from the same limitations as well. In our small patient cohort, we were not able to demonstrate a gain in sensitivity or specificity expected from combined morphologic and functional MR imaging information, compared with ^{18}F-FDG PET/CT. For example, diffusion-weighted imaging, in which malignant lymph nodes are distinctively conspicuous (*28*), did not improve the N staging performance of hybrid ^{18}F-FDG PET/MR imaging in this study.

Although, the mean differences of SUV_{mean} and SUV_{max} of NSCLC derived from ^{18}F-FDG PET/MR imaging and ^{18}F-FDG PET/CT were not statistically significant and exhibited a high correlation. Still, Bland–Altman-analysis revealed that absolute SUV_{mean} and SUV_{max} differs significantly between ^{18}F-FDG PET/MR imaging and ^{18}F-FDG PET/CT. Therefore, quantitative assessment of tumor tissue, for example, in patients evaluated for response to radiation or chemotherapy, has to be interpreted with caution. These differences in absolute standardized uptake values can be influenced by many different factors of technical and biologic nature. In particular, differences between CT-based attenuation correction and MR-based attenuation correction are one potential cause for varying standardized uptake values in ^{18}F-FDG PET/CT and ^{18}F-FDG PET/MR imaging (*29*). However, the PET/MR imaging preserves the clinically relevant image quality in a manner comparable to that of ^{18}F-FDG PET/CT imaging for lesion detection.

In contrast to ^{18}F-FDG PET/CT, simultaneous ^{18}F-FDG PET/MR imaging WB staging can be realized as a 1-stop-shop examination, including the clinically required head MR imaging examination for NSCLC staging. However, the much longer examination time of ^{18}F-FDG PET/MR imaging of approximately 1.5 h is a relevant restraint for clinical practice. It has to be pointed out that for the evaluation of the primary tumor, ^{18}F-FDG PET/CT still is considered as the imaging modality of choice. Although WB ^{18}F-FDG PET/CT provides a high rate in the detection of distant metastases, the use of a hybrid ^{18}F-FDG PET/MR imaging might benefit distant metastases detection, because NSCLC metastases are mainly located in the brain, in the liver, and in the bone. Because MR imaging offers advantages in lesion detection in those tissues, ^{18}F-FDG PET/MR imaging is expected to yield higher detection rates than ^{18}F-FDG PET/CT, whereas ^{18}F-FDG PET/CT is expected to yield higher detection rates in small lung metastases and carcinomatous lymphangiosis. Hence, this study provides a basis for expanded studies to explore the potential advantages of ^{18}F-FDG PET/MR imaging for WB staging in NSCLC patients.

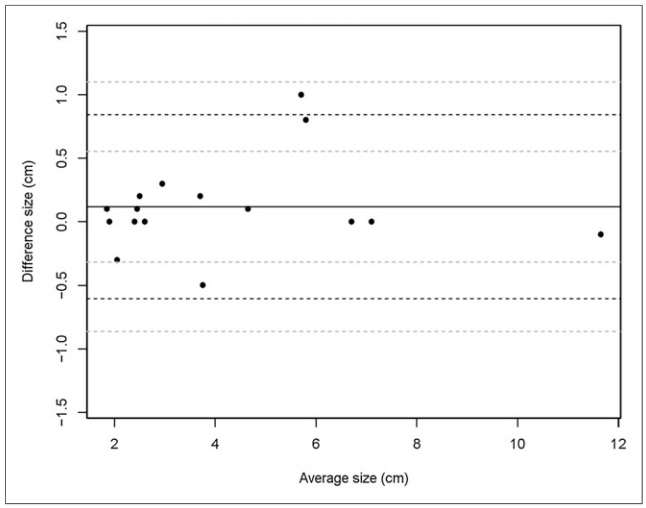

FIGURE 5. Bland–Altman analysis showing lower and upper limits of agreement between ^{18}F-FDG PET/CT and ^{18}F-FDG PET/MR imaging of −0.59 to 0.83 for tumor size.

Admittedly, the number of included patients is relatively low; therefore, these first results have to be considered as preliminary and need further confirmation.

CONCLUSION

^{18}F-FDG PET/MR imaging using a dedicated pulmonary MR imaging protocol, compared with ^{18}F-FDG PET/CT, does not provide advantages in thoracic staging in NSCLC patients.

REFERENCES

1. Jemal A, Bray F, Center MM, Ferlay J, Ward E, Forman D. Global cancer statistics. *CA Cancer J Clin.* 2011;61:69–90.
2. Antoch G, Stattaus J, Nemat AT, et al. Non-small cell lung cancer: dual-modality PET/CT in preoperative staging. *Radiology.* 2003;229:526–533.
3. Kligerman S, Digumarthy S. Staging of non-small cell lung cancer using integrated PET/CT. *AJR.* 2009;193:1203–1211.
4. Cheran SK, Nielsen ND, Patz EF Jr. False-negative findings for primary lung tumors on FDG positron emission tomography: staging and prognostic implications. *AJR.* 2004;182:1129–1132.
5. Nomori H, Watanabe K, Ohtsuka T, Naruke T, Suemasu K, Uno K. Evaluation of F-18 fluorodeoxyglucose (FDG) PET scanning for pulmonary nodules less than 3 cm in diameter, with special reference to the CT images. *Lung Cancer.* 2004; 45:19–27.
6. De Leyn P, Lardinois D, Van Schil PE, et al. ESTS guidelines for preoperative lymph node staging for non-small cell lung cancer. *Eur J Cardiothorac Surg.* 2007;32:1–8.
7. Sommer G, Wiese M, Winter L, et al. Preoperative staging of non-small-cell lung cancer: comparison of whole-body diffusion-weighted magnetic resonance imaging and ^{18}F-fluorodeoxyglucose-positron emission tomography/computed tomography. *Eur Radiol.* 2012;22:2859–2867.
8. Roberts PF, Follette DM, von Haag D, et al. Factors associated with false-positive staging of lung cancer by positron emission tomography. *Ann Thorac Surg.* 2000;70:1154–1159, discussion 9–60.
9. Konishi J, Yamazaki K, Tsukamoto E, et al. Mediastinal lymph node staging by FDG-PET in patients with non-small cell lung cancer: analysis of false-positive FDG-PET findings. *Respiration.* 2003;70:500–506.
10. Tournoy KG, Maddens S, Gosselin R, Van Maele G, van Meerbeeck JP, Kelles A. Integrated FDG-PET/CT does not make invasive staging of the intrathoracic lymph nodes in non-small cell lung cancer redundant: a prospective study. *Thorax.* 2007;62:696–701.
11. Silvestri GA, Gould MK, Margolis ML, et al. Noninvasive staging of non-small cell lung cancer: ACCP evidenced-based clinical practice guidelines (2nd ed.). *Chest*. 2007;132:178S–201S.
12. McLoud TC, Bourgouin PM, Greenberg RW, et al. Bronchogenic carcinoma: analysis of staging in the mediastinum with CT by correlative lymph node mapping and sampling. *Radiology.* 1992;182:319–323.
13. Gould MK, Kuschner WG, Rydzak CE, et al. Test performance of positron emission tomography and computed tomography for mediastinal staging in patients with non-small-cell lung cancer: a meta-analysis. *Ann Intern Med.* 2003; 139:879–892.
14. Kanzaki R, Higashiyama M, Fujiwara A, et al. Occult mediastinal lymph node metastasis in NSCLC patients diagnosed as clinical N0-1 by preoperative integrated FDG-PET/CT and CT: risk factors, pattern, and histopathological study. *Lung Cancer.* 2011;71:333–337.
15. Kim BT, Lee KS, Shim SS, et al. Stage T1 non-small cell lung cancer: preoperative mediastinal nodal staging with integrated FDG PET/CT—a prospective study. *Radiology.* 2006;241:501–509.
16. Billé A, Pelosi E, Skanjeti A, et al. Preoperative intrathoracic lymph node staging in patients with non-small-cell lung cancer: accuracy of integrated positron emission tomography and computed tomography. *Eur J Cardiothorac Surg.* 2009; 36:440–445.
17. Plathow C, Aschoff P, Lichy MP, et al. Positron emission tomography/computed tomography and whole-body magnetic resonance imaging in staging of advanced nonsmall cell lung cancer: initial results. *Invest Radiol.* 2008;43:290–297.
18. Ohno Y, Koyama H, Yoshikawa T, et al. N stage disease in patients with non-small cell lung cancer: efficacy of quantitative and qualitative assessment with STIR turbo spin-echo imaging, diffusion-weighted MR imaging, and fluorodeoxyglucose PET/CT. *Radiology.* 2011;261:605–615.
19. Buchbender C, Heusner TA, Lauenstein TC, Bockisch A, Antoch G. Oncologic PET/MRI, part 2: bone tumors, soft-tissue tumors, melanoma, and lymphoma. *J Nucl Med.* 2012;53:1244–1252.
20. Herzog H, Van Den Hoff J. Combined PET/MR systems: an overview and comparison of currently available options. *Q J Nucl Med Mol Imaging.* 2012; 56:247–267.
21. Antoch G, Bockisch A. Combined PET/MRI: a new dimension in whole-body oncology imaging? *Eur J Nucl Med Mol Imaging.* 2009;36:S113–S120.
22. Schwenzer NF, Schraml C, Muller M, et al. Pulmonary lesion assessment: comparison of whole-body hybrid MR/PET and PET/CT imaging—pilot study. *Radiology.* 2012;264:551–558.
23. Biederer J, Beer M, Hirsch W, et al. MRI of the lung (2/3). Why ... when ... how? *Insights into imaging*. 2012;3:355-71.
24. Shim SS, Lee KS, Kim BT, et al. Non-small cell lung cancer: prospective comparison of integrated FDG PET/CT and CT alone for preoperative staging. *Radiology.* 2005;236:1011–1019.
25. Glazer GM, Gross BH, Quint LE, Francis IR, Bookstein FL, Orringer MB. Normal mediastinal lymph nodes: number and size according to American Thoracic Society mapping. *AJR.* 1985;144:261–265.
26. Yi CA, Shin KM, Lee KS, et al. Non-small cell lung cancer staging: efficacy comparison of integrated PET/CT versus 3.0-T whole-body MR imaging. *Radiology.* 2008;248:632–642.
27. Kohan AA, Kolthammer JA, Vercher-Conejero JL, et al. N staging of lung cancer patients with PET/MRI using a three-segment model attenuation correction algorithm: initial experience. *Eur Radiol.* 2013;23:3161–3169.
28. Nomori H, Mori T, Ikeda K, et al. Diffusion-weighted magnetic resonance imaging can be used in place of positron emission tomography for N staging of non-small cell lung cancer with fewer false-positive results. *J Thorac Cardiovasc Surg.* 2008;135:816–822.
29. Pichler BJ, Kolb A, Nagele T, Schlemmer HP. PET/MRI: paving the way for the next generation of clinical multimodality imaging applications. *J Nucl Med.* 2010;51:333–336.